

Chapter 1

Challenges in Modeling Liquid and Gas Flows in Micro/Nano Devices

Mohamed Gad-el-Hak

Department of Mechanical Engineering

Virginia Commonwealth University, Richmond, VA 23284, U.S.A.

gadelhak@vcu.edu

Traditional fluid mechanics edifies the indifference between liquid and gas flows as long as certain similarity parameters—most prominently the Reynolds number—are matched. This may or may not be the case for flows in nano- or microdevices. The customary continuum, Navier–Stokes modeling is ordinarily applicable for both air and water flowing in macrodevices. Even for common fluids such as air or water, such modeling is bound to fail at sufficiently small scales, but the onset for such failure is different for the two forms of matter. Moreover, when the no-slip, quasi-equilibrium Navier–Stokes system is no longer applicable, the alternative modeling schemes are different for gases and liquids. For dilute gases, statistical methods are applied and the Boltzmann equation is the cornerstone of such approaches. For liquid flows, the dense nature of the matter precludes the use of the kinetic theory of gases, and numerically intensive molecular dynamics simulations are the only alternative rooted in first principles. The present chapter discusses the above issues, emphasizing the differences between liquid and gas transport at the microscale and the physical phenomena unique to liquid flows in minute devices.

Contents

1.1 Introduction	2
1.2 Fluid Mechanics Issues	4
1.3 Fluid Modeling	6
1.4 Gas Flows	9
1.5 Liquid Flows	12
1.6 Molecular Dynamics Simulations	16
1.7 A Typical MD Result	18
1.8 Hybrid Methods	24
1.9 Surface Phenomena	26
1.10 Conclusions	31
References	33

In a little time I felt something alive moving on my left leg, which advancing gently forward over my breast, came almost up to my chin; when bending my eyes downward as much as I could, I perceived it to be a human creature not six inches high, with a bow and arrow in his hands, and a quiver at his back. . . . I had the fortune to break the strings, and wrench out the pegs that fastened my left arm to the ground; for, by lifting it up to my face, I discovered the methods they had taken to bind me, and at the same time with a violent pull, which gave me excessive pain, I a little loosened the strings that tied down my hair on the left side, so that I was just able to turn my head about two inches. . . . These people are most excellent mathematicians, and arrived to a great perfection in mechanics by the countenance and encouragement of the emperor, who is a renowned patron of learning. This prince has several machines fixed on wheels, for the carriage of trees and other great weights.

(From “Gulliver’s Travels—A Voyage to Lilliput,” by Jonathan Swift, 1726.)

In the Nevada desert, an experiment has gone horribly wrong. A cloud of nanoparticles—micro-robots—has escaped from the laboratory. This cloud is self-sustaining and self-reproducing. It is intelligent and learns from experience. For all practical purposes, it is alive. It has been programmed as a predator. It is evolving swiftly, becoming more deadly with each passing hour. Every attempt to destroy it has failed.

And we are the prey.

(From Michael Crichton’s novel “Prey,” HarperCollins Publishers, 2002.)

1.1. Introduction

Almost three centuries apart, the imaginative novelists quoted above contemplated the astonishing, at times frightening possibilities of living beings much bigger or much smaller than us. In 1959, the physicist Richard Feynman envisioned the fabrication of machines minutely small as compared to their makers. Tool making has always differentiated our species from all others on Earth. Aerodynamically correct wooden spears were carved by archaic Homo sapiens close to 400,000 years ago. Man builds things consistent with his size, typically in the range of two orders of magnitude larger or smaller than himself, as indicated in Fig. 1.1. But humans have always striven to explore, build and control the extremes of length and time scales. In the voyages to Lilliput and Brobdingnag of Gulliver’s Travels, Jonathan Swift speculated on the remarkable possibilities which diminution or magnification of physical dimensions provides. The Great Pyramid of Khufu

was originally 147 m high when completed around 2600 B.C., while the Empire State Building, constructed in 1931, is presently—after the addition of a television antenna mast in 1950—449 m high. At the other end of the spectrum of man-made artifacts, a dime is slightly less than 2 cm in diameter. Watchmakers have practised the art of miniaturization since the thirteenth century. The invention of the microscope in the seventeenth century opened the way for direct observation of microbes and plant and animal cells. Smaller things were man-made in the latter half of the twentieth century. The transistor—invented in 1947—in today's integrated circuits has a gate length of 45 nanometers, and approaches 10 nm in research laboratories (source: International Technology Roadmap for Semiconductors <<http://public.itrs.net>>). But what about the miniaturization of mechanical parts—machines—envisioned by Richard Feynman¹ in a legendary lecture delivered in 1959?

Microelectromechanical systems (MEMS) refer to devices that have characteristic length of less than 1 mm but more than 1 micron, that combine electrical and mechanical components, and that are fabricated using integrated circuit batch-processing technologies. MEMS are finding an increasing number of applications in a variety of industrial and medical fields, with a potential worldwide market in the billions of dollars. Accelerometers for automobile airbags, keyless entry systems, dense arrays of micromirrors for high-definition optical displays, scanning electron microscope tips to image single atoms, micro-heat-exchangers for cooling of electronic circuits, reactors for separating biological cells, blood analyzers and pressure sensors for catheter tips are but a few examples of current usage. Microducts are used in infrared detectors, diode lasers, miniature gas chromatographs and high-frequency fluidic control systems. Micropumps are used for ink jet printing, environmental testing and electronic cooling. Potential medical applications for small pumps include controlled delivery and monitoring of minute amount of medication, manufacturing of nanoliters of chemicals and development of artificial pancreas. The much sought-after lab-on-a-chip is promising to automate biology and chemistry to the same extent the integrated circuit has allowed large-scale automation of computation.²

Not all MEMS devices involve fluid flows, but the present paper will focus on the ones that do. Gas flows will first be briefly discussed, but the emphasis of the paper will be on liquid flows. Microducts, micropumps, microturbines, microvalves, microcombustors, synthetic jets and lab-on-a-chip are examples of small devices involving the flow of liquids and gases. Because of length limitation, the present paper only touches on its broad subject matter, with particular emphasis on liquid flows and surface phenomena, and the reader is referred to several other sources for further details.²⁻⁶

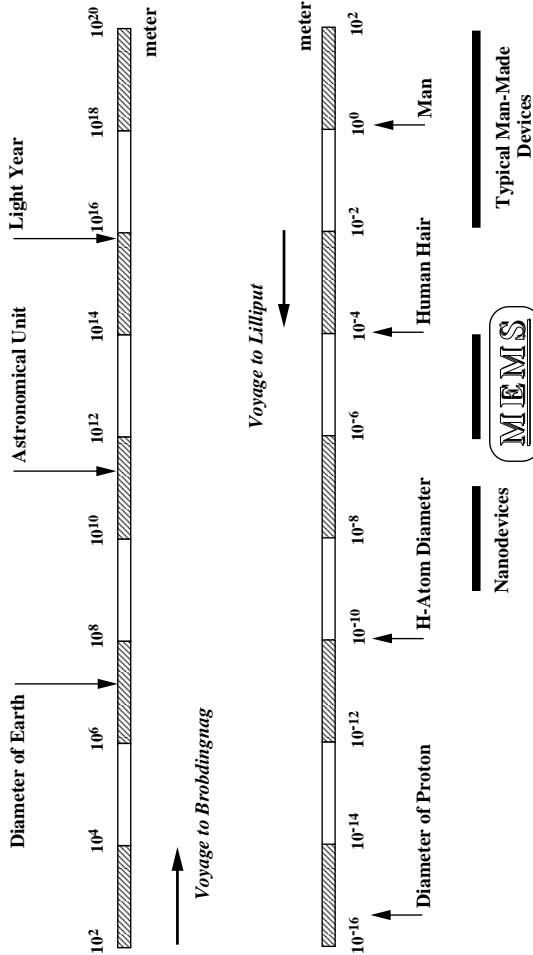


Fig. 1.1. The scale of things in meter. Lower scale continues in the upper bar from left to right. Reproduced with permission from Ref. [3].

1.2. Fluid Mechanics Issues

The rapid progress in fabricating and utilizing microelectromechanical systems during the last decade has not been matched by corresponding advances in our understanding of the unconventional physics involved in the operation and

manufacture of small devices. Providing such understanding is crucial to designing, optimizing, fabricating and operating improved MEMS devices.

Fluid flows in small devices differ from those in macroscopic machines. The operation of MEMS-based ducts, nozzles, valves, bearings, turbomachines, combustors, synthetic jets, *etc.*, cannot always be predicted from conventional flow models such as the Navier–Stokes equations with no-slip boundary condition at a fluid–solid interface, as routinely and successfully applied for larger flow devices. Many questions have been raised when the results of experiments with microdevices could not be explained via traditional flow modeling. The pressure gradient in a long microduct was observed to be non-constant and the measured flowrate was higher than that predicted from the conventional continuum flow model. Slip flow has been observed in microchannels. Load capacities of microbearings were diminished and electric currents needed to move micromotors were extraordinarily high. The dynamic response of micromachined accelerometers operating at atmospheric conditions was observed to be over-damped.

In the early stages of development of this exciting new field, the objective was to build MEMS devices as productively as possible. Microsensors were reading something, but not many researchers seemed to know exactly what. Microactuators were moving, but conventional modeling could not precisely predict their motion. After a decade of unprecedented progress in MEMS technology, perhaps the time is now ripe to take stock, slow down a bit and answer the many questions that arose. The ultimate aim of this long-term exercise is to achieve rational-design capability for useful microdevices and to be able to characterize definitively and with as little empiricism as possible the operations of microsensors and microactuators.

In dealing with fluid flow through microdevices, one is faced with the question of which model to use, which boundary condition to apply and how to proceed to obtain solutions to the problem at hand. Obviously surface effects dominate in small devices. The surface-to-volume ratio for a machine with a characteristic length of 1 m is 1 m^{-1} , while that for a MEMS device having a size of $1 \mu\text{m}$ is 10^6 m^{-1} . The million-fold increase in surface area relative to the mass of the minute device substantially affects the transport of mass, momentum and energy through the surface. The small length scale of microdevices may invalidate the continuum approximation altogether. Slip flow, thermal creep, rarefaction, viscous dissipation, compressibility, intermolecular forces and other unconventional effects may have to be taken into account, preferably using only first principles such as conservation of mass, Newton's second law, and conservation of energy.

In this chapter, I shall discuss liquid flows and surface phenomena. To place the topic in perspective, gas flows in microdevices will first be discussed briefly.

Microfluid mechanics of liquids is more complicated than that for gases. The liquid molecules are much more closely packed at normal pressures and temperatures, and the attractive or cohesive potential between the liquid molecules as well as between the liquid and solid ones plays a dominant role if the characteristic length of the flow is sufficiently small. In cases when the traditional continuum model fails to provide accurate predictions or postdictions, expensive molecular dynamics simulations seem to be the only first-principle approach available to rationally characterize liquid flows in microdevices. Such simulations are not yet feasible for realistic flow extent or number of molecules. As a consequence, the microfluid mechanics of liquids is much less developed than that for gases.

1.3. Fluid Modeling

There are basically two ways of modeling a flowfield. Either as the fluid really is—a collection of molecules—or as a continuum where the matter is assumed continuous and indefinitely divisible. The former modeling is subdivided into deterministic methods and probabilistic ones, while in the latter approach the velocity, density, pressure, *etc.*, are defined at every point in space and time, and conservation of mass, energy and momentum lead to a set of nonlinear partial differential equations (Euler, Navier–Stokes, Burnett, *etc.*). Fluid modeling classification is depicted schematically in Fig. 1.2.

Fluid and heat flows in conventional macrodevices is traditionally modeled using the principles of conservation of mass, momentum (Newton’s second law), and energy (first law of thermodynamics). Additionally, all processes are constrained by the second law of thermodynamics. Those principles are typically expressed in the form of partial differential field equations, where the macroscopic quantities of interest such as velocity, temperature, pressure, *etc.*, depend on a continuum space and time. The first principles, as expressed to describe fluid-transport phenomena in conventional devices, are collectively called the Navier–Stokes equations, a system of nonlinear partial differential equations subject to a sufficient number of initial and boundary conditions, the latter is typically in the form of no velocity slip and no temperature jump at a fluid–solid interface.

There are three fundamental assumptions that must be satisfied in order for the Navier–Stokes equations to be valid:

- The Newtonian framework of mechanics—which specifies that mass and energy are conserved separately and that, in an inertial frame of reference, the sum of all forces is equal to the rate of change of momentum—is valid.

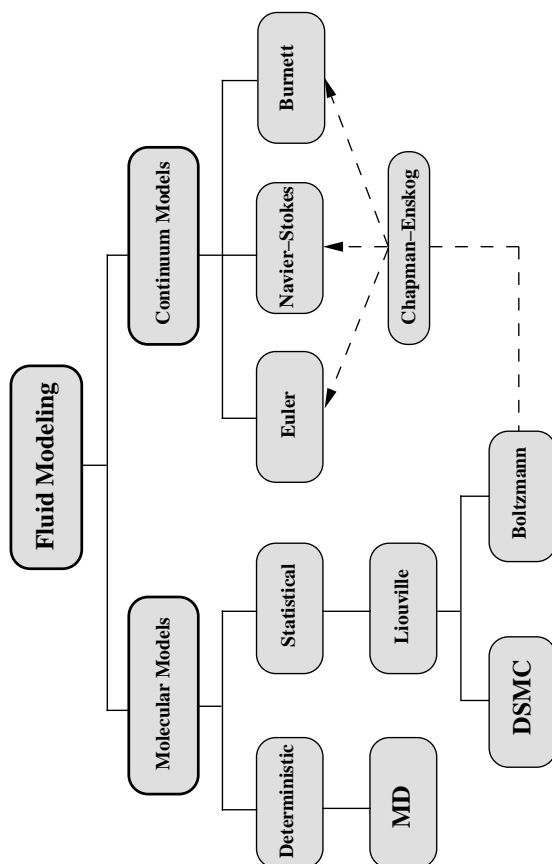


Fig. 1.2. Molecular and continuum flow models. Reproduced with permission from Ref. [3].

- The continuum approximation—which assumes that space and time are indefinitely divisible continuum—is applicable.
- Thermodynamic equilibrium or at least quasi-equilibrium—which permits linear relations between stress and rate of strain and between heat flux and temperature gradient—is assumed.

Fluid isotropy and stress tensor symmetry are also typically, albeit not always, assumed. Violation of any one of the three assumptions listed above invalidates the Navier–Stokes equations and alternative modeling is then called for. We elaborate on the three assumptions in turn.

Newtonian framework: The fluid motions under consideration are assumed non-relativistic, *i.e.*, their characteristic velocities are far below the speed of light. Thus, mass and energy are not interchangeable and each is separately conserved. As long as we are not dealing with atomic or subatomic particles or, at the other extreme of length scale, with stars and galaxies, the Newtonian framework is an excellent modeling tool for most problems in mechanics including those dealing with microelectromechanical systems. Quantum and relativistic mechanics are clearly beyond the scope of the present paper. Therefore, the Newtonian assumption is one that we no longer have to revisit for the rest of this article.

Continuum model: In both solid and fluid mechanics, the continuum approximation implies that the spatial and temporal derivatives of all the macroscopic dependent variables exist in some reasonable sense. In other words, local properties such as density, velocity, stress and heat flux are defined as averages over elements sufficiently large compared with the microscopic structure in order to guarantee a sufficiently large number of molecules inside each fluid element and thus to effect molecular chaos, but small enough in comparison with the scale of the macroscopic phenomena to permit the use of differential calculus to describe those properties. The continuum approximation is almost always met, but exceptions do exist. The resulting equations therefore cover a very broad range of situations, the exception being flows with spatial scales that are not much larger than the mean distance between the fluid molecules, as for example in the case of rarefied gases, shock waves that are thin relative to the molecular distances, and some flows in micro- and nanodevices. We will describe later the precise conditions under which the continuum approximation fails for certain minute devices.

It should be emphasized that the continuum approximation in and by itself leads to an indeterminate set of equations, *i.e.*, more unknowns than equations. To close the resulting system of partial differential equations, relations between the stress and rate of strain and between the heat flux and temperature gradient are needed. At least for compressible flows, two equations of state, relating density and internal energy each to pressure and temperature, are also required. The fact that the continuum approximation does not necessarily lead to the Navier–Stokes equations is a subtle point that is often confused in the literature.

Thermodynamic equilibrium: Thermodynamic equilibrium implies that the macroscopic quantities have sufficient time to adjust to their changing surroundings. In motion, exact thermodynamic equilibrium is impossible as each fluid

particle is continuously having volume, momentum or energy added or removed, and so in fluid dynamics and heat transfer we speak of quasi-equilibrium. The second law of thermodynamics imposes a tendency to revert to equilibrium state, and the defining issue here is whether or not the flow quantities are adjusting fast enough. The reversion rate will be very high if the molecular time and length scales are very small as compared to the corresponding macroscopic flow-scales. This will guarantee that numerous molecular collisions will occur in sufficiently short time to equilibrate fluid particles whose properties vary little over distances comparable to the molecular length scales. For gases, the characteristic length for molecular collision is the mean free path, \mathcal{L} , the average distance traveled by a molecule before colliding with another. When \mathcal{L} is, say, one order of magnitude smaller than the flow length scale, L , macroscopic quantities such as velocity and temperature will have nearly linear gradients over molecular distances, and it is on these gradients alone that departure from equilibrium will depend. Therefore, the quasi-equilibrium assumption signifies that the stress is linearly related to the rate of strain (Newtonian fluids) and the heat flux is linearly related to the temperature gradient (Fourier fluids). These issues have been described quite eloquently by Lighthill.⁸ Thermodynamic equilibrium additionally gives rise to the no-slip and no-temperature-jump boundary conditions.^{8,9}

As is the case with the continuum approximation, the quasi-equilibrium assumption can be violated under certain circumstances relevant to microdevices. In these cases, alternatives to the no-slip condition or even to the Navier–Stokes equations themselves must be sought. We are now ready to quantify the conditions under which the continuum approximation or the quasi-equilibrium assumption can be made. For gases at least, the answer to both questions is well known from statistical thermodynamics particularly as was extensively applied to rarefied gas dynamics half a century ago.^{9,10} For that reason we discuss gas flows first deferring the discussion of liquid flows to afterward.

1.4. Gas Flows

The well-known chart reproduced in Fig. 1.3 clearly illustrates the answer we are seeking. All scales in this plot are logarithmic. The bottom abscissa represents the density normalized with a reference density, ρ/ρ_0 , or equivalently the normalized number density (number of molecules per unit volume), n/n_0 . The top abscissa is the average distance between molecules normalized with the molecular diameter, δ/σ . Clearly, the density ratio is proportional to the inverse cube of δ/σ . The left ordinate represents a characteristic flow dimension, L , in meter. This can be computed from a characteristic macroscopic property, such as density, divided by

the absolute value of its gradient. The right ordinate is the length scale normalized with the molecular diameter, L/σ . The chart in Fig. 1.3 depicts a gas having a molecular diameter of $\sigma = 4 \times 10^{-10}$ m, which diameter very closely represents air modeled as rigid spheres. Similar charts can be drawn for other gases.

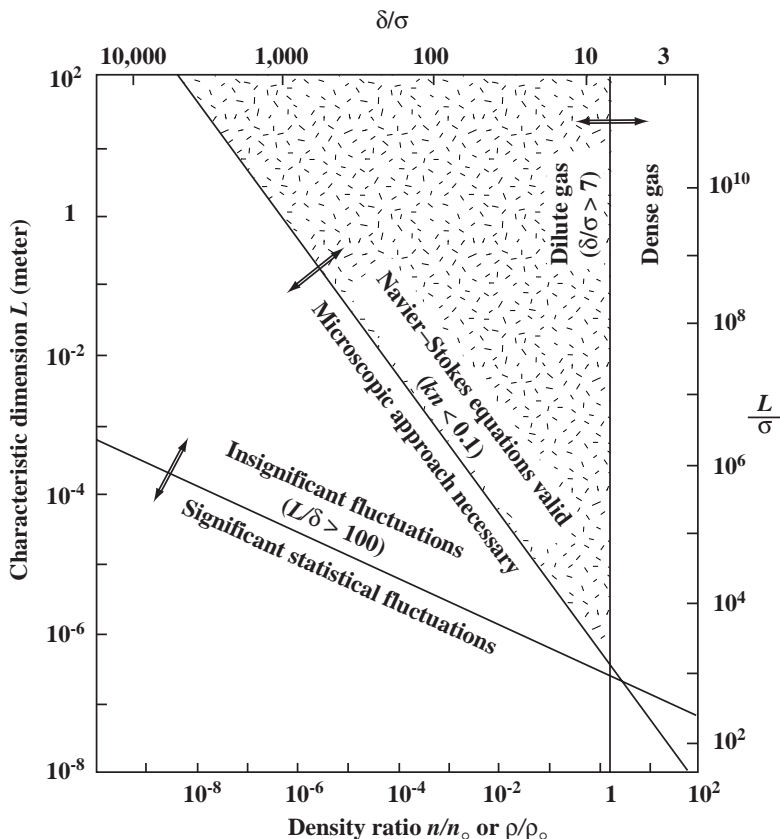


Fig. 1.3. Effective limits of different flow models. Reproduced with permission from Ref. [10].

The vertical line inserted in Fig. 1.3 represents the boundary between dilute gas and dense one. Dilute gas is to the left of this line where $\delta/\sigma > 7$. For such gas, intermolecular forces play no role and the molecules spend most of their time in free flight between brief collisions at which instances the molecules' direction and speed abruptly change. Additionally, the probability of more than two molecules colliding is minuscule. We then speak of only binary collisions,

and all the simplifications of the powerful kinetic theory of gases can be invoked when dealing with dilute gases. Dry air at standard conditions has a pressure of $1.01 \times 10^5 \text{ N/m}^2$, temperature of 288 K, density ratio of 1, and $\delta/\sigma = 9$. Standard air is therefore a dilute, ideal gas, but barely.

The gently sloped line in Fig. 1.3 indicates the limit of molecular chaos. When averaging over many molecules to compute macroscopic quantities, insignificant statistical fluctuations occur when there is at least 100 molecules to the side $L/\sigma > 100$, in other words when at least 1 million molecules reside inside the smallest macroscopic fluid volume of interest. Therefore, the continuum approximation is valid only on top of that line. The molecular chaos restriction improves the accuracy of computing the macroscopic quantities from the microscopic information. In essence, the volume over which averages are computed has to have sufficient number of molecules to reduce statistical errors. It can be shown that computing macroscopic flow properties by averaging over a number of molecules will result in statistical fluctuations with a standard deviation of approximately 0.1% if one million molecules are used, around 3% if one thousand molecules are used, and so on.

The steeper line in Fig. 1.3 indicates the boundary of validity of the quasi-equilibrium assumption. This limit is governed by the Knudsen number, $\text{Kn} \equiv \mathcal{L}/L$, which is the ratio of the mean free path to the characteristic macroscopic length. Navier–Stokes equations are valid only if $\text{Kn} < 0.1$ (above the steeper line), although the no-slip condition demands the stricter limit of $\text{Kn} < 0.001$. The line corresponding to the stricter limit is parallel to the steeper line in Fig. 1.3 but shifted upward by two decades. The mean free path is proportional to n^{-1} , and therefore the slope of the quasi-equilibrium line, in the logarithmic plot, is three times steeper than that of the molecular chaos line. Much of that has been known since the classical experiments conducted by Knudsen.¹¹ These experiments have been recently repeated with great precision at the U.S. National Institute of Standards and Technology by Tison¹² and reported by Beskok *et al.*¹³

How does all that relate to microdevices? As density is reduced, the gas changes from dense to dilute. As size shrinks for a low-density gas, the flow slips, followed by a failure of the Navier–Stokes equation, followed by a failure of the continuum approximation altogether. For a dense gas, a reverse trend is observed as L is reduced: the continuum approximation fails first followed by a failure of the quasi-equilibrium assumption. Clearly, the continuum approximation and the quasi-equilibrium assumption are two different things. The two lines in Fig. 1.3 describing the two respective limits meet only at a single point.

To give a concrete example, for air at 1 atm, slip occurs if $L < 100$ microns, (stress)–(rate of strain) relation becomes nonlinear if $L < 1$ micron, and the

continuum approximation fails altogether if $L < 0.4$ micron. For air at 10^{-3} atm, slip occurs if $L < 100$ nm, (stress)–(rate of strain) relation becomes nonlinear if $L < 1$ μm , and the continuum approximation fails if $L < 4$ microns. Light gases such as Helium will reach those limits at considerably larger characteristic lengths. All of those conditions are well within the operating ranges of micro- and nanodevices. Thus, there are circumstances when transport in microdevices should not be modeled using the traditional equations.

The next step for both gas and liquid flows is to figure out what to do if conventional modeling fails. For gases at least, there are first-principles equations that give the precise amount of slip or temperature jump to include in case the Knudsen number exceeds the critical limit of 0.001.³ Higher-order equations such as those of Burnett can replace the Navier–Stokes equations when Kn exceeds 0.1. Finally, if the continuum approximation fails altogether, the fluid can be modeled as it really is, a collection of molecules. There, one can use molecular dynamics simulations (for liquids), Boltzmann equation (for dilute gases), or direct simulations Monte Carlo (also for dilute gases). Subject to their own limitations, all the molecular-based models can also be used in lieu of higher-order momentum and energy equations, *i.e.*, for non-equilibrium, continuum situations. All the strategies listed here are schematically depicted in Fig. 1.2, and described in greater details in the books by Karniadakis and Beskok⁶ and Gad-el-Hak.⁵

1.5. Liquid Flows

From the continuum point of view, liquids and gases are both fluids obeying the same equations of motion. For incompressible flows, for example, the Reynolds number is the primary dimensionless parameter that determines the character of the flowfield for a given geometry. True, water, for example, has density and viscosity that are, respectively, three and two orders of magnitude higher than those for air, but if the Reynolds number and geometry are matched, liquid and gas flows should be identical.^a For MEMS applications, however, we anticipate the possibility of non-equilibrium flow conditions and the consequent invalidity of the Navier–Stokes equations and the no-slip boundary conditions. Such circumstances can best be researched using the molecular approach. This was discussed for gases in the previous section, and the corresponding arguments for liquids will be given in the present section. The literature on non-Newtonian fluids in general and polymers in particular is vast (for example, the bibliographic survey by Nadolink and Haigh¹⁴ cites over 4,900 references on polymer drag reduction

^aBarring phenomena unique to liquids such as cavitation, free surface flows, *etc.*

alone) and provides a rich source of information on the molecular approach for liquid flows.

Solids, liquids and gases are distinguished merely by the degree of proximity and the intensity of motions of their constituent molecules. In solids, the molecules are packed closely and confined, each hemmed in by its neighbors.⁹ Only rarely would one solid molecule slip from its neighbors to join a new set. As the solid is heated, molecular motion becomes more violent and a slight thermal expansion takes place. At a certain temperature that depends on ambient pressure, sufficiently intense motion of the molecules enables them to pass freely from one set of neighbors to another. The molecules are no longer confined but are nevertheless still closely packed, and the substance is now considered a liquid. Further heating of the matter eventually releases the molecules altogether, allowing them to break the bonds of their mutual attractions. Unlike solids and liquids, the resulting gas expands to fill any volume available to it.

Unlike solids, both liquids and gases cannot resist finite shear force without continuous deformation; that is the definition of a fluid medium. In contrast to the reversible, elastic, static deformation of a solid, the continuous deformation of a fluid resulting from the application of a shear stress results in an irreversible work that eventually becomes random thermal motion of the molecules; that is viscous dissipation. There are around 25 million molecules of STP air in a one-micron cube. The same cube would contain around 34 billion molecules of water. So, liquid flows are continuum even in extremely small devices through which gases would not be considered continuum. The average distance between molecules in the gas example is one order of magnitude higher than the diameter of its molecules, while that for the liquid phase approaches the molecular diameter. As a result, liquids are almost incompressible. Their isothermal compressibility coefficient α and bulk expansion coefficient β are much smaller compared to those for gases. For water, for example, a hundred-fold increase in pressure leads to less than 0.5% decrease in volume. Sound speeds through liquids are also high relative to those for gases, and as a result most liquid flows are incompressible.^b Notable exceptions to that are propagation of ultra-high-frequency sound waves and cavitation phenomena.

The mechanisms through which liquids transport mass, momentum and energy must be very different from those of gases. In dilute gases, intermolecular forces play no role and the molecules spend most of their time in free flight between brief collisions at which instances the molecules' direction and speed abruptly change. The random molecular motions are responsible for gaseous transport

^bNote that we distinguish between a fluid and a flow being compressible/incompressible. For example, the flow of the highly compressible air can be either compressible or incompressible.

processes. In liquids, on the other hand, the molecules are closely packed though not fixed in one position. In essence, the liquid molecules are always in a collision state. Applying a shear force must create a velocity gradient so that the molecules move relative to one another, *ad infinitum* as long as the stress is applied. For liquids, momentum transport due to the random molecular motion is negligible compared to that due to the intermolecular forces. The straining between liquid molecules causes some to separate from their original neighbors, bringing them into the force field of new molecules. Across the plane of the shear stress, the sum of all intermolecular forces must, on the average, balance the imposed shear. Liquids at rest transmit only normal force, but when a velocity gradient occurs, the net intermolecular force will have a tangential component.

The incompressible Navier–Stokes equations describe liquid flows under most circumstances. But what are the conditions for which the no-slip Navier–Stokes equations fail to adequately describe liquid flows? In other words, how small does a device have to be before a particular liquid flow starts slipping perceptibly and for the stress–strain relation to become nonlinear? Answering this question from first principles is the holy grail of microfluidic modeling. Liquids do not have a well-advanced molecular-based theory as that for dilute gases. The concept of mean free path is not very useful for liquids and the conditions under which a liquid flow fails to be in quasi-equilibrium state are not well defined. There is no Knudsen number for liquid flows to guide us through the maze. We do not know, from first principles, the conditions under which the no-slip boundary condition becomes inaccurate, or the point at which the (stress)–(rate of strain) relation or the (heat flux)–(temperature gradient) relation fails to be linear. Certain empirical observations indicate that those simple relations that we take for granted occasionally fail to accurately model liquid flows. For example, it has been shown in rheological studies¹⁵ that non-Newtonian behavior commences when the strain rate approximately exceeds twice the molecular frequency-scale

$$\dot{\gamma} = \frac{\partial u}{\partial y} \geq 2\mathfrak{S}^{-1} \quad (1.1)$$

where the molecular time scale \mathfrak{S} is given by

$$\mathfrak{S} = \left[\frac{m\sigma^2}{\epsilon} \right]^{\frac{1}{2}} \quad (1.2)$$

where m is the molecular mass, and σ and ϵ are respectively the characteristic length and energy scales for the molecules. For ordinary liquids such as water, this time scale is extremely small and the threshold shear rate for the onset of

non-Newtonian behavior is therefore extraordinarily high. For high-molecular-weight polymers, on the other hand, m and σ are both many orders of magnitude higher than their respective values for water, and the linear stress–strain relation breaks down at realistic values of the shear rate.

As is the case for gas flows, the threshold for the occurrence of measurable slip in liquid flows is expected to be higher (in terms of, say, channel height) than that necessary for the occurrence of nonlinear stress–strain relation. The moving contact line when a liquid spreads on a solid substrate is an example where slip flow must be allowed to avoid singular or unrealistic behavior in the Navier–Stokes solutions.^{16–19} Other examples where slip-flow must be admitted include corner flows^{20,21} and extrusion of polymer melts from capillary tubes.^{22–24} Wall slip in polymer extrusion is discussed extensively by Den.²⁵ The recent chapter by Lauga, Brenner and Stone²⁶ provides a comprehensive treatment of the no-slip boundary condition for Newtonian and non-Newtonian fluids as well as for polar and non-polar liquids. These authors trace the issue to its 19th century roots, and survey both the experimental and analytical aspects of the problem.

Existing experimental results of liquid flow in microdevices are contradictory. This is not surprising given the difficulty of such experiments and the lack of a guiding rational theory. References [27–30] summarize the relevant literature. For small-length-scale flows, a phenomenological approach for analyzing the data is to define an apparent viscosity μ_a calculated so that if it were used in the traditional no-slip Navier–Stokes equations instead of the actual fluid viscosity μ , the results would be in agreement with experimental observations. Israelachvili³¹ and Gee *et al.*³² found that $\mu_a = \mu$ for thin-film flows as long as the film thickness exceeds 10 molecular layers (≈ 5 nm). For thinner films, μ_a depends on the number of molecular layers and can be as much as 10^5 times larger than μ . Chan and Horn's results³³ are somewhat different: the apparent viscosity deviates from the fluid viscosity for films thinner than 50 nm.

In polar-liquid flows through capillaries, Migun and Prokhorenko³⁴ report that μ_a increases for tubes smaller than 1 micron in diameter. In contrast, Debye and Cleland³⁵ report μ_a smaller than μ for paraffin flow in porous glass with average pore size several times larger than the molecular length scale. Experimenting with microchannels ranging in depths from 0.5 micron to 50 microns, Pfahler *et al.*²⁷ found that μ_a is consistently smaller than μ for both liquid (isopropyl alcohol; silicone oil) and gas (nitrogen; helium) flows in microchannels. For liquids, the apparent viscosity decreases with decreasing channel depth. Other researchers using small capillaries report that μ_a is about the same as μ .^{36–41}

More recently, Sharp⁴² and Sharp *et al.*⁴³ asserted that, despite the significant inconsistencies in the literature regarding liquid flows in microchannels, such

flows are well predicted by macroscale continuum theory. A case can be made to the contrary, however, as will be seen at the end of Section 1.7, and the final verdict on this controversy is yet to come.

The above contradictory results point to the need for replacing phenomenological models by first-principles ones. The lack of molecular-based theory of liquids—despite extensive research by the rheology and polymer communities—leaves molecular dynamics simulations (MD) as the nearest weapon to first-principles arsenal. MD simulations offer a unique approach to checking the validity of the traditional continuum assumptions. However, as was pointed out earlier, such simulations are limited to exceedingly minute flow extent. Koplik and Banavar²¹ offer a useful primer on the history, principles, applications and limitations of molecular dynamics simulations. We provide in the following section a brief discussion of MD simulations.

1.6. Molecular Dynamics Simulations

The molecular models recognize the fluid as a myriad of discrete particles: molecules, atoms, ions and electrons. The goal here is to determine the position, velocity and state of all particles at all times. The molecular approach is either deterministic or probabilistic (refer to Fig. 1.2), and the former is the most fundamental of the molecular approaches. The motion of the molecules are governed by the laws of classical mechanics, although, at the expense of greatly complicating the problem, the laws of quantum mechanics can also be considered in special circumstances. The modern molecular dynamics computer simulations have been pioneered by Alder and Wainwright,^{44–46} and reviewed by Ciccotti and Hoover,⁴⁷ Allen and Tildesley,⁴⁸ Haile,⁴⁹ and Koplik and Banavar.²¹

The MD simulation begins with a set of N molecules in a region of space, each assigned a random velocity corresponding to a Boltzmann distribution at the temperature of interest. The interaction between the particles is prescribed typically in the form of a two-body potential energy and the time evolution of the molecular positions is determined by integrating Newton's equations of motion, one for each molecule. Because MD is based on the most basic set of equations, it is valid in principle for any flow extent and any range of parameters. The method is straightforward in principle but there are two hurdles: choosing a proper and convenient potential for particular fluid and solid combinations, and the colossal computer resources required to simulate a reasonable flowfield extent. A significant advantage of molecular dynamics simulations is that the relation between the stress and rate of strain as well as between the heat flux and temperature gradient comes out as part of the answer. In other words, whether the fluid is Newtonian/

non-Newtonian or Fourier/non-Fourier does not have to be assumed. Likewise, the presence/absence of momentum or energy slip at a solid wall comes out as part of the answer. The issue of thermodynamic equilibrium or lack thereof is therefore moot.

For purists, the difficulty of choosing a potential is a sticky one. Aside from computer-intensive quantum mechanics calculations, there is currently no totally rational methodology by which a convenient potential can be favored. Part of the art of molecular dynamics simulations is to pick an appropriate potential and validate the simulation results with experiments or other analytical/computational results. By astutely choosing the potential and its parameters, one can essentially obtain any desired result; a clear weakness of the MD approach. A commonly used potential between two molecules is the generalized Lennard-Jones 6–12 potential, to be used and further discussed in the sections.

The second difficulty, and by far the most serious limitation of molecular dynamics simulations, is the number of molecules N that can realistically be modeled on a digital computer. Since the computation of an element of trajectory for any particular molecule requires consideration of all other molecules as potential collision partners, the amount of computation required by the MD method is proportional to N^2 . Some saving in computer time can be achieved by cutting off the weak tail of the potential (see Fig. 1.4) at, say, $r_c = 2.5\sigma$, and shifting the potential by a linear term in r so that the force goes smoothly to zero at the cutoff. As a result, only nearby molecules are treated as potential collision partners, and the computation time for N molecules no longer scales with N^2 .

The state of the art of molecular dynamics simulations in the early 2000s is such that with a few hours of CPU time, general-purpose supercomputers can handle around 100,000 molecules. At enormous expense, the fastest parallel machine available can simulate around 10 million particles, although more recent reports of an order-of-magnitude higher number of molecules have been made (MIT's Nicolas G. Hadjiconstantinou; private communication). Because of the extreme diminution of molecular scales, the 10 million figure translates into regions of liquid flow of about 0.06 mm (600 Angstroms) in linear size, over time intervals of around 0.001 ms, enough for continuum behavior to set in for simple molecules. To simulate 1 s of real time for complex molecular interactions, *e.g.*, including vibration modes, reorientation of polymer molecules, collision of colloidal particles, *etc.*, requires unrealistic CPU time measured in hundreds of years.

MD simulations are highly inefficient for dilute gases where the molecular interactions are infrequent. The simulations are more suited for dense gases and liquids. Clearly, molecular dynamics simulations are reserved for situations where the continuum approach or the statistical methods are inadequate to compute from

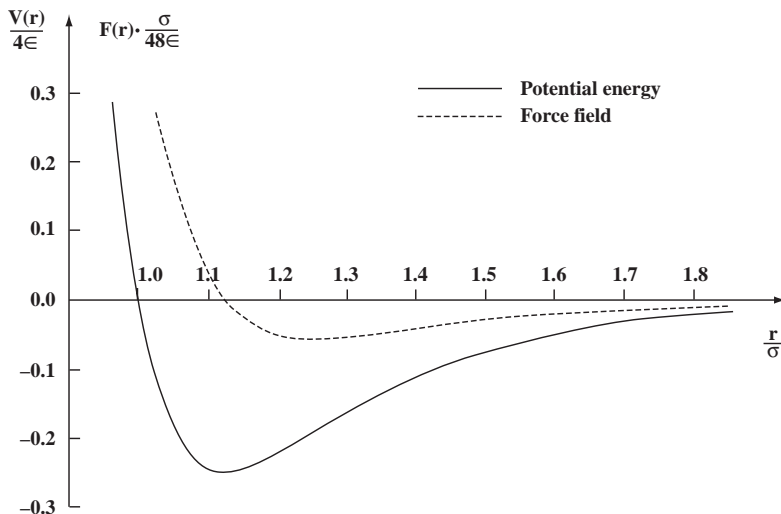


Fig. 1.4. Typical Lennard-Jones 6–12 potential and the intermolecular force field resulting from it. Only a small portion of the potential function is shown for clarity.

first principles important flow quantities. Slip boundary condition for a liquid flow in an extremely small device is such a case, as will be discussed in the following section.

1.7. A Typical MD Result

Thompson and Troian⁵⁰ provide molecular dynamics simulations to quantify the slip-flow boundary condition dependence on shear rate. Recall the linear Navier boundary condition introduced⁵¹ in 1823,

$$\Delta u|_w = u_{\text{fluid}} - u_{\text{wall}} = L_s \left. \frac{\partial u}{\partial y} \right|_w \quad (1.3)$$

where L_s is the constant slip length, and $(\partial u / \partial y)|_w$ is the strain rate computed at the wall. The goal of Thompson and Troian's simulations was to determine the degree of slip at a solid–liquid interface as the interfacial parameters and the shear rate change. In their simulations, a simple liquid underwent planar shear in a Couette cell as shown in Fig. 1.5. The typical cell measured $12.51 \times 7.22 \times h$, in units of molecular length scale σ , where the channel depth h varied in the range of 16.71σ – 24.57σ , and the corresponding number of molecules simulated ranged from 1,152 to 1,728. The liquid is treated as an isothermal ensemble of

spherical molecules. A shifted Lennard-Jones 6–12 potential is used to model intermolecular interactions, with energy and length scales ϵ and σ , and cut-off distance $r_c = 2.2\sigma$:

$$V(r) = 4\epsilon \left[\left(\frac{r}{\sigma}\right)^{-12} - \left(\frac{r}{\sigma}\right)^{-6} - \left(\frac{r_c}{\sigma}\right)^{-12} + \left(\frac{r_c}{\sigma}\right)^{-6} \right] \quad (1.4)$$

The truncated potential is set to zero for $r > r_c$.

The fluid–solid interaction is also modeled with a truncated Lennard-Jones potential, with energy and length scales ϵ^{wf} and σ^{wf} , and cut-off distance r_c . The equilibrium state of the fluid is a well-defined liquid phase characterized by number density $n = 0.81\sigma^{-3}$ and temperature $T = 1.1\epsilon/k$, where k is the Boltzmann constant.

The steady state velocity profiles resulting from Thompson and Troian’s MD simulations⁵⁰ are depicted in Fig. 1.5 for different values of the interfacial parameters ϵ^{wf} , σ^{wf} and n^w . Those parameters, shown in units of the corresponding fluid parameters ϵ , σ and n , characterize, respectively, the strength of the liquid–solid coupling, the thermal roughness of the interface and the commensurability of wall and liquid densities. The macroscopic velocity profiles recover the expected flow behavior from continuum hydrodynamics with boundary conditions involving varying degrees of slip. Note that when slip exists, the shear rate $\dot{\gamma}$ no longer equals U/h . The degree of slip increases (*i.e.*, the amount of momentum transfer at the wall–fluid interface decreases) as the relative wall density n^w increases or the strength of the wall–fluid coupling σ^{wf} decreases; in other words when the relative surface energy corrugation of the wall decreases. Conversely, the corrugation is maximized when the wall and fluid densities are commensurate and the strength of the wall–fluid coupling is large. In this case, the liquid feels the corrugations in the surface energy of the solid owing to the atomic close-packing. Consequently, there is efficient momentum transfer and the no-slip condition applies, or in extreme cases, a ‘stick’ boundary condition takes hold.

Variations of the slip length L_s and viscosity μ as functions of shear rate $\dot{\gamma}$ are shown in parts (a) and (b) of Fig. 1.6, for five different sets of interfacial parameters. For Couette flow, the slip length is computed from its definition, $\Delta u|_w / \dot{\gamma} = (U/\dot{\gamma} - h) / 2$. The slip length, viscosity and shear rate are normalized in the figure using the respective molecular scales for length, viscosity, and inverse time. The viscosity of the fluid is constant over the entire range of shear rates (Fig. 1.6b), indicating Newtonian behavior. As indicated earlier, non-Newtonian behavior is expected for $\dot{\gamma} \geq 2\mathfrak{S}^{-1}$, well above the shear rates used in Thompson and Troian’s simulations.

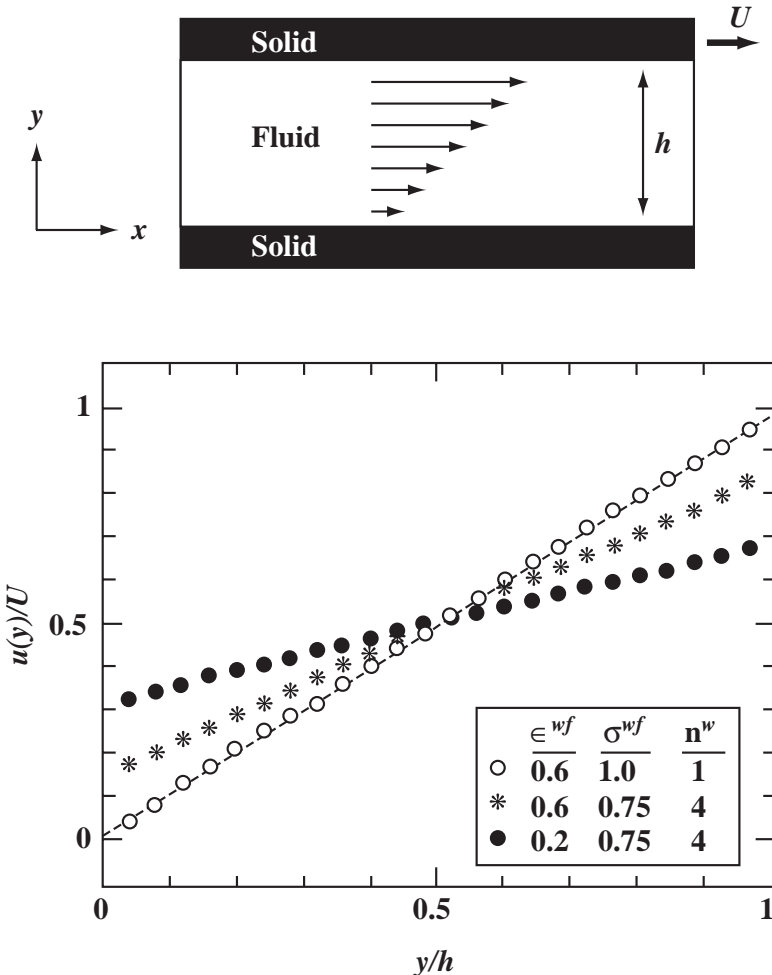


Fig. 1.5. Velocity profiles in a Couette flow geometry at different interfacial parameters. All three profiles are for $U = \sigma\mathfrak{S}^{-1}$, and $h = 2,457\sigma$. The dashed line is the no-slip Couette-flow solution. Reproduced with permission from Ref. [50].

At low shear rates, the slip length behavior is consistent with the Navier model, *i.e.*, is independent of the shear rate. Its limiting value ranges from 0 to $\sim 17\sigma$ for the range of interfacial parameters chosen (Fig. 1.6a). In general, the amount of slip increases with decreasing surface energy corrugation. Most interestingly, at high shear rates the Navier condition breaks down as the slip length increases rapidly with $\dot{\gamma}$. The critical shear-rate value for the slip length to diverge, $\dot{\gamma}_c$,

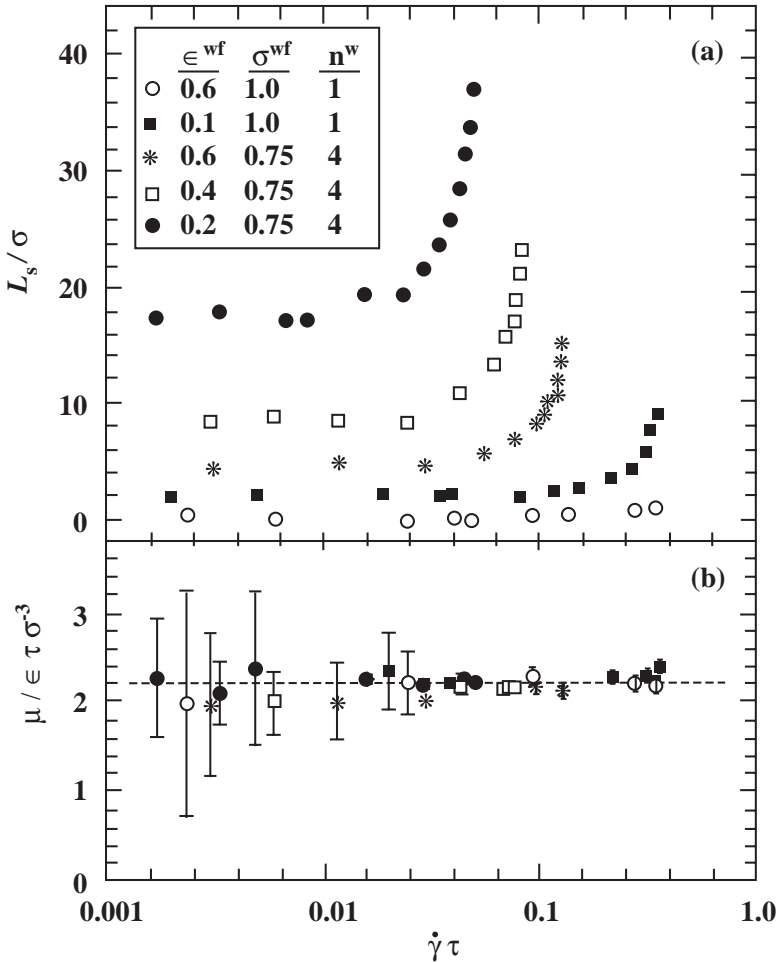


Fig. 1.6. Variation of slip length and viscosity as functions of shear rate. Reproduced with permission from Ref. [50].

decreases as the surface energy corrugation decreases. Surprisingly, the boundary condition is nonlinear even though the liquid is still Newtonian. In dilute gases, the linear slip condition and the Navier–Stokes equations, with their linear stress–strain relation, are both valid to the same order of approximation in Knudsen number. In other words, deviation from linearity is expected to take place at the same value of $Kn = 0.1$. In liquids, in contrast, the slip length appears to become nonlinear and to diverge at a critical value of shear rate well below the shear

rate at which the linear stress–strain relation fails. Moreover, the boundary condition deviation from linearity is not gradual but is rather catastrophic. The critical value of shear rate $\dot{\gamma}_c$ signals the point at which the solid can no longer impart momentum to the liquid. This means that the same liquid molecules sheared against different substrates will experience varying amounts of slip and vice versa.

Based on the above results, Thompson and Troian⁵⁰ suggest a universal boundary condition at a solid–liquid interface. Scaling the slip length L_s by its asymptotic limiting value L_s^o and the shear rate $\dot{\gamma}$ by its critical value $\dot{\gamma}_c$, collapses the data in the single curve shown in Fig. 1.7. The data points are well described by the relation

$$L_s = L_s^o \left[1 - \frac{\dot{\gamma}}{\dot{\gamma}_c} \right]^{-\frac{1}{2}} \quad (1.5)$$

The nonlinear behavior close to a critical shear rate suggests that the boundary condition can significantly affect flow behavior at macroscopic distances from the wall. Experiments with polymers confirm this observation.⁵² The rapid change in the slip length suggests that for flows in the vicinity of $\dot{\gamma}_c$, small changes in surface properties can lead to large fluctuations in the apparent boundary condition. Thompson and Troian⁵⁰ conclude that the Navier slip condition is but the low-shear-rate limit of a more generalized universal relationship which is nonlinear and divergent. Their relation provides a mechanism for relieving the stress singularity in spreading contact lines and corner flows, as it naturally allows for varying degrees of slip on approach to regions of higher rate of strain.

To place the above results in physical terms, consider water^c at a temperature of $T = 288$ K. The energy-scale in the Lennard-Jones potential is then $\epsilon = 3.62 \times 10^{-21}$ J. For water, $m = 2.99 \times 10^{-26}$ kg, $\sigma = 2.89 \times 10^{-10}$ m, and at standard temperature $n = 3.35 \times 10^{28}$ molecules/m³. The molecular time-scale can thus be computed,

$$\mathfrak{S} = [m \sigma^2 / \epsilon]^{1/2} = 8.31 \times 10^{-13} \text{ s} \quad (1.6)$$

For the third case depicted in Fig. 1.7 (the open squares), $\dot{\gamma}_c \mathfrak{S} = 0.1$, and the critical shear rate at which the slip condition diverges is thus $\dot{\gamma}_c = 1.2 \times 10^{11} \text{ s}^{-1}$.

^cWater molecules are complex ones, forming directional, short-range covalent bonds. Thus requiring a more complex potential than the Lennard-Jones to describe the intermolecular interactions. For the purpose of the qualitative example described here, however, we use the computational results of Thompson and Troian (1997) who employed the L-J potential.

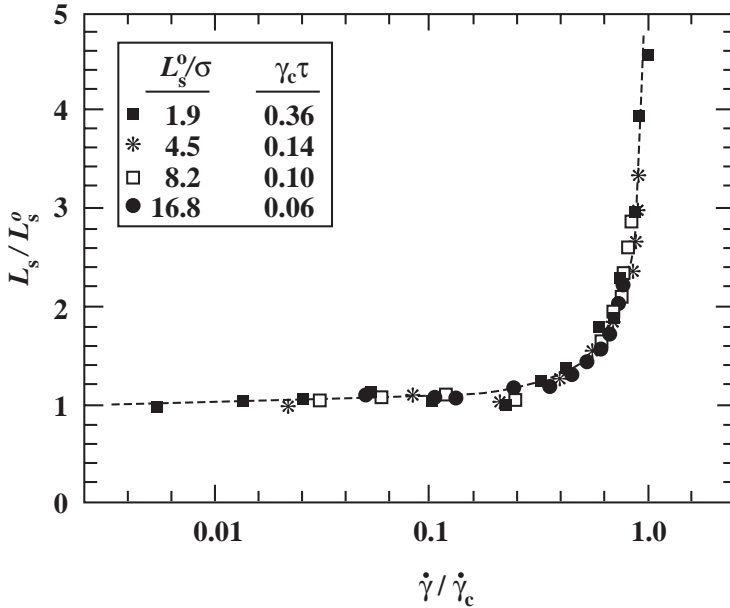


Fig. 1.7. Universal relation of slip length as a function of shear rate. Reproduced with permission from Ref. [50].

Such an enormous rate of strain^d may be found in extremely small devices having extremely high speeds. On the other hand, the conditions to achieve a measurable slip of 17σ (the solid circles in Fig. 1.6) are not difficult to encounter in microdevices: density of solid four times that of liquid, and energy-scale for wall–fluid interaction that is one fifth of energy-scale for liquid.

The limiting value of slip length is independent of the shear rate and can be computed for water as $L_s^o = 17\sigma = 4.91 \times 10^{-9}$ m. Consider a water microbearing having a shaft diameter of $100 \mu\text{m}$ and rotation rate of 20,000 rpm and a minimum gap of $h = 1 \mu\text{m}$. In this case, $U = 0.1$ m/s and the no-slip shear rate is $U/h = 10^5 \text{ s}^{-1}$. When slip occurs at the limiting value just computed, the shear rate and the wall slip-velocity are computed as follows:

$$\dot{\gamma} = \frac{U}{h + 2L_s^o} = 9.90 \times 10^4 \text{ s}^{-1} \quad (1.7)$$

$$\Delta u \Big|_w = \dot{\gamma} L_s = 4.87 \times 10^{-4} \text{ m/s.} \quad (1.8)$$

^dNote however that $\dot{\gamma}_c$ for high-molecular-weight polymers would be many orders of magnitude smaller than the value developed here for water.

As a result of the Navier slip, the shear rate is reduced by 1% from its no-slip value, and the slip velocity at the wall is about 0.5% of U , small but not insignificant.

1.8. Hybrid Methods

At sufficiently small device scale for both liquid and gas flows, the continuum and the quasi-equilibrium hypotheses eventually fail or at least yield increasingly inaccurate results. This is true even for simple fluids such as air or water where non-equilibrium effects, *e.g.*, velocity slip, temperature jump, non-Newtonian and non-Fourier behavior, are not ordinarily observed in macrodevices operating near room pressure and temperature. Because of widely different molecular spacings, the scale at which the traditional assumptions should no longer be made clearly differs for dilute gases and for dense gases and liquids.

Noting the difficulty of obtaining reliable experimental data at the micro/nano scales, the no-slip Navier–Stokes equations themselves should not be used to determine the scale at which those assumptions fail to provide accurate modeling of the flow under consideration, as that is clearly a circular argument. The kinetic theory of dilute gases provides powerful answers, and enables us to determine from first principles the scales at which the no-slip assumption, the linear stress–rate of strain relation, and the continuum hypothesis are no longer valid. Note that those three assumptions fail at progressively smaller device size, much the same as they do fail at progressively lower density or higher altitude. For dense gases and liquids, on the other hand, no such straightforward strategy as the kinetic theory exists, first to answer the question of whether or not the Navier–Stokes system is usable, and second to provide a more accurate alternative.

A molecular dynamics simulation offers a first-principles solution to the problem, but is limited to unrealistically small spatial and temporal scales. For example, the time step needed to simulate pure water with fixed O–H bonds and H–O–H angles is dictated by the fastest frequency needed to be resolved and is of the order of 2 fs. To simulate a mere 1 ms of real time, a whopping 500 million time steps are needed, requiring well above one year of CPU time. The physical phenomena investigated in a typical microdevice occur over a broad range of spatial and temporal scales. One way out of this conundrum is to use a hybrid method, where the expensive, high-resolution atomistic model is confined to flow regions in which it is needed, *e.g.*, near strong flow gradients and fluid–solid interfaces, and the continuum model is used in the rest of the computational domain. Such hybrid methods can in principle be used in solids,^{53–55} dilute gases,^{56–64} and liquids.^{65–71} In all cases, however, the challenge is to choose the correct coupling

method and to properly match the interface between the atomistic and continuum regions. Coupling is done based on the physics of the particular flow problem investigated (whether the continuum flow is compressible or incompressible; steady or unsteady), and is considered more or less a solved problem.^{69,70} On the other hand, passing information from the continuum to the molecular subdomain is a more subtle problem that at present has no satisfactory solution for dense gases and liquids. This is caused by our inability to unambiguously define and recreate the interacting molecular state for a dense gas (or a liquid) from knowledge of the continuum solution, which is essentially the first few moments of the non-equilibrium distribution function (Nicolas G. Hadjiconstantinou; private communication).

For dilute gases, the atomistic calculation of choice is the Boltzmann equation simulation tool known as the direct simulation Monte Carlo (DSMC).⁶⁹ Baker and Hadjiconstantinou⁷² assert that considerable saving in computational time can be achieved by considering only the deviation from thermodynamic equilibrium. This is particularly important in the low Mach number limit where DSMC is slow to converge as it computes the Boltzmann collision integral. In this Mach number limit, important for typical MEMS flows, the deviation from equilibrium is modest and quicker convergence of the statistical sampling of macroscopic observables such as flow velocity is achieved by Baker and Hadjiconstantinou's variance reduction technique.

Continuum–DSMC hybrid methods allows the simulation of complex phenomena at the microscale without the prohibitive cost of a purely atomistic calculation. The two computational regimes are matched over a region of space where both are assumed to be valid. For compressible flows, the continuum and atomistic time steps are comparable, and explicit time integration with a finite-volume-type coupling technique is feasible. The adaptive mesh and algorithm refinement (AMAR) scheme proposed by Wijesinghe *et al.*⁷⁰ provides a robust flux-based method for coupling an atomistic fluid representation to a continuum model. The algorithm extends adaptive mesh refinement by introducing the molecular description at the finest level of refinement. This is not possible generally for incompressible, dilute gas flows, as explicit integration at the molecular time step becomes prohibitive. An implicit method, based on a domain decomposition approach known as the Schwarz alternating method, has been successfully demonstrated by Wijesinghe and Hadjiconstantinou.⁶⁹ This coupling method uses state variables instead of fluxes to achieve the matching, and provides time-scale decoupling between the very small atomistic time and the much larger Courant–Friedrich–Lewy (CFL) stability time step in the stiff continuum calculations. Convergence to the global problem steady state is reached via iteration between the steady state

solutions of the continuum and atomistic subdomains. Imposition of the boundary conditions on the molecular simulations is accomplished by extending the molecular subdomain through the artifice of a reservoir region in which molecules are generated using a Chapman–Enskog distribution that is parametrized by the Navier–Stokes flow field in the continuum subdomain.

For dense gases and liquids, molecular dynamics simulations are used in the very near proximity of rigid or compliant walls, while the Navier–Stokes equations are discretized in the bulk of the flow.⁷⁰ As mentioned earlier, the outstanding difficulty in such hybrid simulation is passing the information from the continuum to the molecular subdomain. We are simply unable to unambiguously define and recreate the liquid interacting molecular state from knowledge of the continuum solution. In that case, heuristic approaches inevitably replace first-principles strategies. Very recently, Werder *et al.*⁷¹ proposed an MD simulation coupled to a finite volume discretization of the N–S equations. The two descriptions were combined in a domain decomposition formulation using the Schwarz alternating method. The method avoids direct imposition of fluxes but ensures flux continuity by matching the transport coefficients in the overlap region. Non-periodic velocity boundary conditions were imposed from the continuum to the atomistic domain based on an effective boundary potential, consistent body forces, particle insertion algorithm and specular walls. The strategy iteratively finds a consistent solution in the atomistic and continuum domains. An overlap region heuristically facilitates information exchange between the two subdomains in the form of state (Dirichlet) boundary conditions. Convergence is reached in successive Schwarz iterations when the solutions in the continuum and atomistic subdomains become identical in the overlap region. This technique was applied to the flow of liquid argon around a carbon nanotube and the resulting flow field was found to agree with a fully atomistic reference solution.

1.9. Surface Phenomena

The surface-to-volume ratio for a machine with a characteristic length of 1 m is 1 m^{-1} , while that for a MEMS device having a size of $1 \mu\text{m}$ is 10^6 m^{-1} . The million-fold increase in surface area relative to the mass of the minute device substantially affects the transport of mass, momentum and energy through the surface. Obviously surface effects dominate in small devices. The surface boundary conditions in MEMS flows have been discussed above and in the extensive literature cited in Refs. [26] and [73]. In microdevices, it has been shown that it is possible to have measurable slip-velocity and temperature jump at a solid–fluid interface. Liquids such as macromolecule polymers would slip even in minichannels (mm

scale).²⁵ In this section, we illustrate other ramifications of the large surface-to-volume ratio unique to MEMS, and provide a molecular viewpoint to surface forces.

In microdevices, both radiative and convective heat loss/gain are enhanced by the huge surface-to-volume ratio. Consider a device having a characteristic length L_s . Use of the lumped capacitance method to compute the rate of convective heat transfer, for example, is justified if the Biot number ($\equiv h L_s / \kappa_s$, where h is the convective heat transfer coefficient of the fluid and κ_s is the thermal conductivity of the solid) is less than 0.1. Small L_s implies small Biot number, and a nearly uniform temperature within the solid. Within this approximation, the rate at which heat is lost to the surrounding fluid is given by

$$\rho_s L_s^3 c_s \frac{dT_s}{dt} = -h L_s^2 (T_s - T_\infty) \quad (1.9)$$

where ρ_s and c_s are respectively the density and specific heat of the solid, T_s is its (uniform) temperature, and T_∞ is the ambient fluid temperature. Solution of the above equation is trivial, and the temperature of a hot surface drops exponentially with time from an initial temperature T_i ,

$$\frac{T_s(t) - T_\infty}{T_i - T_\infty} = \exp\left[-\frac{t}{\mathcal{T}}\right] \quad (1.10)$$

where the time constant \mathcal{T} is given by

$$\mathcal{T} = \frac{\rho_s L_s c_s}{h} \quad (1.11)$$

For small devices, the time it takes the solid to cool down is proportionally small. Clearly, the million-fold increase in surface-to-volume ratio implies a proportional increase in the rate at which heat escapes. Identical scaling arguments can be made regarding mass transfer.

Another effect of the diminished scale is the increased importance of surface forces and the waning importance of body forces. Based on biological studies, Went⁷⁴ concludes that the demarcation length scale is around 1 mm. Below that, surface forces dominate over gravitational forces. A 10 mm piece of paper will fall down when gently placed on a smooth, vertical wall, while a 0.1 mm piece will stick. Try it! *Stiction* is a major problem in MEMS applications. Certain structures such as long, thin polysilicon beams and large, thin comb drives have a propensity to stick to their substrates and thus fail to perform as designed.^{75,76}

Conventional dry friction between two solids in relative motion is proportional to the normal force which is usually a component of the moving device weight. The friction is independent of the contact-surface area because the van der Waals cohesive forces are negligible relative to the weight of the macroscopic device. In MEMS applications, the cohesive intermolecular forces between two surfaces are significant and the stiction is independent of the device mass but is proportional to its surface area. The first micromotor did not move—despite large electric current through it—until the contact area between the 100 micron rotor and the substrate was reduced significantly by placing dimples on the rotor's surface.^{77–79}

One last example of surface effects that to my knowledge has not been investigated for microflows is the adsorbed layer in gaseous wall-bounded flows. It is well known^{8,80} that when a gas flows in a duct, the gas molecules are attracted to the solid surface by the van der Waals and other forces of cohesion. The potential energy of the gas molecules drops on reaching the surface. The adsorbed layer partakes the thermal vibrations of the solid, and the gas molecules can only escape when their energy exceeds the potential energy minimum. In equilibrium, at least part of the solid would be covered by a monomolecular layer of adsorbed gas molecules. Molecular species with significant partial pressure—relative to their vapor pressure—may locally form layers two or more molecules thick. Consider, for example, the flow of a mixture of dry air and water vapor at STP. The energy of adsorption of water is much larger than that for nitrogen and oxygen, making it more difficult for water molecules to escape the potential energy trap. It follows that the life time of water molecules in the adsorbed layer significantly exceeds that for the air molecules (by 60,000 folds, in fact) and, as a result, the thin surface layer would be mostly water. For example, if the proportion of water vapor in the ambient air is 1:1,000 (*i.e.*, very low humidity level), the ratio of water to air in the adsorbed layer would be 60:1. Microscopic roughness of the solid surface causes partial condensation of the water along portions having sufficiently strong concave curvature. So, surfaces exposed to non-dry airflows are mainly liquid water surfaces. In most applications, this thin adsorbed layer has little effect on the flow dynamics, despite the fact that the density and viscosity of liquid water are far greater than those for air. In MEMS applications, however, the layer thickness may not be an insignificant portion of the characteristic flow dimension and the water layer may have a measurable effect on the gas flow. A hybrid approach of molecular dynamics and continuum flow simulations or MD–Monte Carlo simulations may be used to investigate this issue.

It should be noted that recently, Majumdar and Mezic^{81,82} have studied the stability and rupture into droplets of thin liquid films on solid surfaces. They point out that the free energy of a liquid film consists of a surface tension component

as well as highly nonlinear volumetric intermolecular forces resulting from van der Waals, electrostatic, hydration and elastic strain interactions. For water films on hydrophilic surfaces such as silica and mica, Majumdar and Mezic⁸¹ estimate the equilibrium film thickness to be about 0.5 nm (2 monolayers) for a wide range of ambient-air relative humidities. The equilibrium thickness grows very sharply, however, as the relative humidity approaches 100%.

Majumdar and Mezic's results^{81,82} open many questions. What are the stability characteristics of their water film in the presence of airflow above it? Would this water film affect the accommodation coefficient for microduct airflow? In a modern Winchester-type hard disk, the drive mechanism has a read/write head that floats 50 nm above the surface of the spinning platter. The head and platter together with the air layer in between form a slider bearing. Would the computer performance be affected adversely by the high relative humidity on a particular day when the adsorbed water film is no longer 'thin'? If a microduct hauls liquid water, would the water film adsorbed by the solid walls influence the effective viscosity of the water flow? Electrostatic forces can extend to almost 1 micron (the Debye length), and that length is known to be highly pH-dependent. Would the water flow be influenced by the surface and liquid chemistry? Would this explain the contradictory experimental results of liquid flows in microducts discussed earlier?

The few examples above illustrate the importance of surface effects in small devices. From the continuum viewpoint, forces at a solid–fluid interface are the limit of pressure and viscous forces acting on a parallel elementary area displaced into the fluid, when the displacement distance is allowed to tend to zero. From the molecular point of view, all macroscopic surface forces are ultimately traced to intermolecular forces, which subject is extensively covered in the book by Israelachvili⁸³ and references therein. Here we provide a very brief introduction to the molecular viewpoint. The four forces in nature are (i) the strong and (ii) weak forces describing the interactions between neutrons, protons, electrons, *etc.*; (iii) the electromagnetic forces between atoms and molecules; and (iv) gravitational forces between masses. The range of action of the first two forces is around 10^{-5} nm, and hence neither concerns us overly in MEMS applications. The electromagnetic forces are effective over a much larger though still small distance on the order of the inter-atomic separations (0.1–0.2 nm). Effects over longer range—several orders of magnitude longer—can and do rise from the short-range intermolecular forces. For example, the rise of liquid column in capillaries and the action of detergent molecules in removing oily dirt from fabric are the result of intermolecular interactions. Gravitational forces decay with the distance to second power, while intermolecular forces decay much quicker, typically with the seventh power. Cohesive forces are therefore negligible once the distance between

molecules exceeds few molecular diameters, while massive bodies like stars and planets are still strongly interacting, via gravity, over astronomical distances.

Electromagnetic forces are the source of all intermolecular interactions and the cohesive forces holding atoms and molecules together in solids and liquids. They can be classified into (i) purely electrostatic arising from the Coulomb force between charges, interactions between charges, permanent dipoles, quadrupoles, *etc.*; (ii) polarization forces arising from the dipole moments induced in atoms and molecules by the electric field of nearby charges and permanent dipoles; and (iii) quantum mechanical forces that give rise to covalent or chemical bonding and to repulsive steric or exchange interactions that balance the attractive forces at very short distances. The Hellman–Feynman theorem of quantum mechanics states that once the spatial distribution of the electron clouds has been determined by solving the appropriate Schrödinger equation, intermolecular forces may be calculated on the basis of classical electrostatics, in effect reducing all intermolecular forces to Coulombic forces. Note however that intermolecular forces exist even when the molecules are totally neutral. Solutions of the Schrödinger equation for general atoms and molecules are not easy of course, and alternative modeling are sought to represent intermolecular forces. The van der Waals attractive forces are usually represented with a potential that varies as the inverse-sixth power of distance, while the repulsive forces are represented with either a power or an exponential potential.

A commonly used potential between two molecules is the generalized Lennard-Jones (L-J 6–12) pair potential given by

$$V_{ij}(r) = 4\epsilon \left[c_{ij} \left(\frac{r}{\sigma} \right)^{-12} - d_{ij} \left(\frac{r}{\sigma} \right)^{-6} \right] \quad (1.12)$$

where V_{ij} is the potential energy between two particles i and j , r is the distance between the two molecules, ϵ and σ are respectively characteristic energy- and length-scales, and c_{ij} and d_{ij} are parameters to be chosen for the particular fluid and solid combinations under consideration. The first term in the right-hand side is the strong repulsive force that is felt when two molecules are at extremely close range comparable to the molecular length-scale. That short-range repulsion prevents overlap of the molecules in physical space. The second term is the weaker, van der Waals attractive force that commences when the molecules are sufficiently close (several times σ). That negative part of the potential represents the attractive polarization interaction of neutral, spherically symmetric particles. The power of 6 associated with this term is derivable from quantum mechanics considerations, while the power of the repulsive part of the potential is found empirically. The

Lennard-Jones potential is zero at very large distances, has a weak negative peak at r slightly larger than σ , is zero at $r = \sigma$, and is infinite as $r \rightarrow 0$.

The force field resulting from this potential is given by

$$F_{ij}(r) = -\frac{\partial V_{ij}}{\partial r} = \frac{48\epsilon}{\sigma} \left[c_{ij} \left(\frac{r}{\sigma}\right)^{-13} - \frac{d_{ij}}{2} \left(\frac{r}{\sigma}\right)^{-7} \right] \quad (1.13)$$

A typical L-J 6-12 potential and force field was shown in Fig. 1.4, for $c = d = 1$. The minimum potential $V_{\min} = -\epsilon$, corresponds to the equilibrium position (zero force) and occurs at $r = 1.12\sigma$. The attractive van der Waals contribution to the minimum potential is -2ϵ , while the repulsive energy contribution is $+\epsilon$. Thus the inverse 12th-power repulsive force term decreases the strength of the binding energy at equilibrium by 50%.

The L-J potential is commonly used in molecular dynamics simulations to model intermolecular interactions between dense gas or liquid molecules and between fluid and solid molecules. As mentioned earlier, such potential is not accurate for complex substances such as water whose molecules form directional covalent bonds. As a result, MD simulations for water are much more involved.

1.10. Conclusions

The traditional Navier–Stokes model of fluid flows with no-slip boundary conditions works only for a certain range of the governing parameters. This model basically demands three conditions: (i) Newtonian mechanics, and not quantum or relativistic mechanics, applies; (ii) The fluid is a continuum, which is typically satisfied as there are usually more than 1 million molecules in the smallest volume in which appreciable macroscopic changes take place. This is the molecular chaos restriction, which can be violated for rarefied gas flows in macrodevices or for STP airflows in nanodevices; and (iii) The flow is not too far from thermodynamic equilibrium, which is satisfied if there is sufficient number of molecular encounters during a time period small compared to the smallest time scale for flow changes. During this time period the average molecule would have moved a distance small compared to the smallest flow length scale.

For gases, the Knudsen number determines the degree of rarefaction and the applicability of traditional flow models. As $\text{Kn} \rightarrow 0$, the time and length scales of molecular encounters are vanishingly small compared to those for the flow, and the velocity distribution of each element of the fluid instantaneously adjusts to the equilibrium thermodynamic state appropriate to the local macroscopic properties as this molecule moves through the flowfield. From the continuum viewpoint, the flow is isentropic and heat conduction and viscous diffusion and dissipation

vanish from the continuum conservation relations, leading to the Euler equations of motion. At small but finite Kn , the Navier–Stokes equations describe quasi-equilibrium, continuum flows.

Slip flow must be taken into account for $Kn > 0.001$. The slip boundary condition is at first linear in Knudsen number, then nonlinear effects take over beyond a Knudsen number of 0.1. At the same transition regime, *i.e.*, $0.1 < Kn < 10$, the linear stress–rate of strain and heat flux–temperature gradient relations—needed to close the field equations—also break down, and alternative continuum equations (*e.g.*, Burnett or higher-order equations) or molecular-based models must be invoked. In the transition regime, provided that the dilute gas and molecular chaos assumptions hold, solutions to the difficult Boltzmann equation are sought, but physical simulations such as Monte Carlo methods are more readily executed in this range of Knudsen number. In the free-molecule flow regime, *i.e.*, $Kn > 10$, the nonlinear collision integral is negligible and the Boltzmann equation is drastically simplified. Analytical solutions are possible in this case for simple geometries and numerical integration of the Boltzmann equation is straightforward for arbitrary geometries, provided that the surface-reflection characteristics are accurately modeled.

Gaseous flows are often compressible in microdevices even at low Mach numbers. Viscous effects can cause sufficient pressure drop and density changes for the flow to behave as compressible. In a long, constant-area microduct, all Knudsen number regimes may be encountered and the degree of rarefaction increases along the tube. The pressure drop is nonlinear and the Mach number increases downstream, limited only by choked-flow condition.

Similar deviation and breakdown of the traditional Navier–Stokes equations occur for liquids as well, but at considerably smaller device scale. Existing experiments are contradictory, and the situation for dense gases and liquids is more murky than that for dilute gases. There is no kinetic theory of liquids, and first-principles prediction methods are scarce. Molecular dynamics simulations can be used, but they are limited to extremely small flow extents. Nevertheless, measurable slip is predicted from MD simulations at realistic shear rates in microdevices. Hybrid atomistic–continuum methods hold promise to provide first-principles solutions while remaining computationally affordable. Though requiring considerable numerical erudition, the use of hybrid strategies for dilute gases is within reach. Further development is needed for implementing hybrid methods for liquid and dense gas flows.

Much non-traditional physics is still to be learned and many exciting applications of microdevices are yet to be discovered. The future is bright for this emerging field of nanoscience and nanotechnology.

References

1. R. P. Feynman, There's plenty of room at the bottom, in *Miniaturization*, ed. H. D. Gilbert, pp. 282–296, New York: Reinhold Publishing (1961).
2. T. M. Squires, S. R. Quake, Microfluidics: fluid physics at the nanoliter scale. *Rev. Mod. Phys.* **77**, 977–1026 (2005).
3. M. Gad-el-Hak, The fluid mechanics of microdevices—the Freeman scholar lecture”. *J. Fluids Eng.* **121**, 5–33 (1999).
4. H. A. Stone, A. D. Stroock, A. Ajdari, Engineering flows in small devices: microfluidics toward a lab-on-a-chip. *Annu. Rev. Fluid Mech.* **36**, 381–411 (2004).
5. M. Gad-el-Hak, ed., *The MEMS Handbook*, second edition, volumes I–III, Boca Raton: CRC Press (2005).
6. G. Em Karniadakis, A. Beskok, *Microflows: Fundamentals and Simulation*, New York: Springer-Verlag (2002).
7. G. K. Batchelor, *An Introduction to Fluid Dynamics*, London: Cambridge University Press (1967).
8. M. J. Lighthill, Introduction. Real and ideal fluids, in *Laminar Boundary Layers*, ed. L. Rosenhead, pp. 1–45, Oxford: Clarendon Press (1963).
9. S. Chapman, T. G. Cowling, *The Mathematical Theory of Non-Uniform Gases*, third edition, London: Cambridge University Press (1970).
10. G. A. Bird, *Molecular Gas Dynamics and the Direct Simulation of Gas Flows*, Oxford: Clarendon Press (1994).
11. M. Knudsen, Die gesetze der molekularströmung und der inneren reibungsströmung der gase durch röhren. *Annalen der Physik* **28**, 75–130 (1909).
12. S. A. Tison, Experimental data and theoretical modeling of gas flows through metal capillary leaks. *Vacuum* **44**, 1171–1175 (1993).
13. A. Beskok, G. E. Karniadakis, W. Trimmer, Rarefaction and compressibility effects in gas microflows. *J. Fluids Eng.* **118**, 448–456 (1996).
14. R. H. Nadolink, W. W. Haigh, Bibliography on skin friction reduction with polymers and other boundary-layer additives. *Appl. Mech. Rev.* **48**, 351–459 (1995).
15. W. Loose, S. Hess, Rheology of dense fluids via nonequilibrium molecular hydrodynamics: shear thinning and ordering transition. *Rheologica Acta* **28**, 91–101 (1989).
16. E. B. Dussan, S. H. Davis, On the motion of fluid–fluid interface along a solid surface. *J. Fluid Mech.* **65**, 71–95 (1974).
17. E. B. Dussan, The moving contact line: the slip boundary condition. *J. Fluid Mech.* **77**, 665–684 (1976).
18. E. B. Dussan, On the spreading of liquids on solid surfaces: static and dynamic contact lines. *Annu. Rev. Fluid Mech.* **11**, 371–400 (1976).
19. P. A. Thompson, M. O. Robbins, Simulations of contact line motion: slip and the dynamic contact angle. *Phys. Rev. Lett.* **63**, 766–769 (1989).
20. H. K. Moffatt, Viscous and resistive eddies near a sharp corner. *J. Fluid Mech.* **18**, 1–18 (1964).
21. J. Koplik, J. R. Banavar, Continuum deductions from molecular hydrodynamics. *Annu. Rev. Fluid Mech.* **27**, 257–292 (1995).
22. J. R. A. Pearson, C. J. S. Petrie, On melt flow instability of extruded polymers, in *Polymer Systems: Deformation and Flow*, eds. R. E. Wetton, R. W. Whorlow, pp. 163–187, London: Macmillan (1968).

23. S. Richardson, On the no-slip boundary condition. *J. Fluid Mech.* **59**, 707–719 (1973).
24. M. M. Den, Issues in viscoelastic fluid mechanics. *Annu. Rev. Fluid Mech.* **22**, 13–34 (1990).
25. M. M. Den, Extrusion instabilities and wall slip. *Annu. Rev. Fluid Mech.* **33**, 265–287 (2001).
26. E. Lauga, M. P. Brenner, H. A. Stone, Microfluidics: the no-slip boundary condition, in *Handbook of Experimental Fluid Dynamics*, eds. J. Foss, C. Tropea, A. Yarin, chapter 15, New York: Springer (2006).
27. J. Pfahler, J. Harley, H.H. Bau, J.N. Zemel, Liquid transport in micron and submicron channels. *Sensors and Actuators* **21–23**, 431–434 (1990).
28. J. Pfahler, J. Harley, H. H. Bau, J. N. Zemel, Gas and liquid flow in small channels, in *Proc. Symp. on Micromechanical Systems, Sensors, and Actuators*, eds. D. Cho, R. Warrington, A. Pisano, H. H. Bau, C. Friedrich, J. Jara-Almonte, J. Liburdy, ASME DSC-Vol. 32, pp. 49–60, New York: ASME (1991).
29. J. Pfahler, Liquid transport in micron and submicron size channels, Ph.D. Thesis, University of Pennsylvania, Philadelphia, Pennsylvania (1992).
30. H. H. Bau, Transport processes associated with micro-devices. *Thermal Sci. Eng.* **2**, 172–178 (1994).
31. J. N. Israelachvili, Measurement of the viscosity of liquids in very thin films. *J. Colloid Interface Sci.* **110**, 263–271 (1986).
32. M. L. Gee, P. M. McGuiggan, J. N. Israelachvili, A. M. Homola, Liquid to solidlike transitions of molecularly thin films under shear. *J. Chemical Phys.* **93**, 1895–1906 (1990).
33. D. Y. C. Chan, R. G. Horn, Drainage of thin liquid films. *J. Chemical Phys.* **83**, 5311–5324 (1985).
34. N. P. Migun, P. P. Prokhorenko, Measurement of the viscosity of polar liquids in microcapillaries. *Colloid J. of the USSR* **49**, 894–897 (1987).
35. P. Debye, R. L. Cleland, Flow of liquid hydrocarbons in porous Vycor. *J. Appl. Phys.* **30**, 843–849 (1959).
36. J. L. Anderson, J. A. Quinn, Ionic mobility in microcapillaries. *J. Chemical Phys.* **27**, 1208–1209 (1972).
37. D. B. Tuckermann, R. F. W. Pease, High-performance heat sinking for VLSI. *IEEE Electron Device Lett.* **EDL-2**, 126–129 (1981).
38. D. B. Tuckermann, R. F. W. Pease, Optimized convective cooling using micromachined structures. *J. Electrochemical Soc.* **129**, C98, March (1982).
39. D. B. Tuckermann, Heat transfer microstructures for integrated circuits, Ph.D. Thesis, Stanford University, Palo Alto, California (1984).
40. M. G. Guvenc, V-groove capillary for low flow control and measurement, in *Micro-machining and Micropackaging of Transducers*, eds. C. D. Fung, P. W. Cheung, W. H. Ko, D. G. Fleming, pp. 215–223, Amsterdam: Elsevier (1985).
41. S. Nakagawa, S. Shoji, M. Esashi, A micro-chemical analyzing system integrated on silicon chip, in *Proc. IEEE: Micro Electro Mechanical Systems*, Napa Valley, California, IEEE 90CH2832-4, New York: IEEE (1990).
42. K. V. Sharp, Experimental investigation of liquid and particle-laden flows in microtubes, Ph.D. Thesis, University of Illinois at Urbana–Champaign (2001).

43. K. V. Sharp, R. J. Adrian, J. G. Santiago, J. I. Molho, Liquid flow in microchannels, in *The MEMS Handbook*, vol. I, second edition, ed. M. Gad-el-Hak, pp. 10.1–10.45, Boca Raton: CRC Press (2006).
44. B. J. Alder, T. E. Wainwright, Studies in molecular dynamics. *J. Chemical Phys.* **27**, 1208–1209 (1957).
45. B. J. Alder, T. E. Wainwright, Molecular dynamics by electronic computers, in *Transport Processes in Statistical Mechanics*, ed. I. Prigogine, pp. 97–131, New York: Interscience (1958).
46. B. J. Alder, T. E. Wainwright, Decay of the velocity auto-correlation function. *Phys. Rev. A* **1**, 18–21 (1970).
47. G. Ciccotti, W. G. Hoover, eds., *Molecular Dynamics Simulation of Statistical Mechanics Systems*, Amsterdam: North Holland (1986).
48. M. P. Allen, D. J. Tildesley, *Computer Simulation of Liquids*, Oxford: Clarendon Press (1987).
49. J. M. Haile, *Molecular Dynamics Simulation: Elementary Methods*, New York: Wiley (1993).
50. P. A. Thompson, S. M. Troian, A general boundary condition for liquid flow at solid surfaces. *Nature* **389**, 360–362 (1997).
51. C. L. M. H. Navier, Mémoire sur les lois du mouvement des fluides. *Mémoires de l'Académie Royale des Sciences de l'Institut de France* **VI**, 389–440 (1823).
52. B. T. Atwood, W. R. Schowalter, Measurements of slip at the wall during flow of high-density polyethylene through a rectangular conduit. *Rheologica Acta* **28**, 134–146 (1989).
53. F. F. Abraham, J. Q. Broughton, N. Bernstein, E. Kaxiras, Spanning the continuum to quantum length scales in a dynamic simulation of brittle fracture. *Europhys. Lett.* **44**, 783–787 (1998).
54. V. B. Shenoy, R. Miller, E. B. Tadmor, D. Rodney, R. Phillips, M. Ortiz, An adaptive finite element approach to atomic-scale mechanics—the quasicontinuum method. *J. Mech. Phys. Solids* **47**, 611–642 (1999).
55. R. E. Rudd, J. Q. Broughton, Concurrent coupling of length scales in solid state systems. *Physica Status Solidi B* **217**, 251–291 (2000).
56. D. C. Wadsworth, D. A. Erwin, One-dimensional hybrid continuum/particle simulation approach for rarefied hypersonic flows. AIAA Paper Number 90-1690 (1990).
57. D. Hash, H. Hassan, A decoupled DSMC/Navier–Stokes analysis of a transitional flow experiment. AIAA Paper Number 96-353 (1996).
58. J. Bourgat, P. Le Tallec, M. Tidriri, Coupling Boltzmann and Navier–Stokes equations by friction. *J. Comput. Phys.* **127**, 227–245 (1996).
59. B. J. Alder, Highly discretized dynamics. *Physica A* **240**, 193–195 (1997).
60. P. Le Tallec, F. Mallinger, Coupling Boltzmann and Navier–Stokes Equations by half fluxes. *J. Comput. Phys.* **136**, 51–67 (1997).
61. S. Tiwari, A. Klar, Coupling of the Boltzmann and Euler equations with adaptive domain decomposition procedure. *J. Comput. Phys.* **144**, 710–726 (1998).
62. A. L. Garcia, J. Bell, W. Y. Crutchfield, B. J. Alder, Adaptive mesh and algorithm refinement using direct simulation Monte Carlo. *J. Comput. Phys.* **154**, 134–155 (1999).
63. O. Aktas, N. R. Aluru, A combined continuum/DSMC technique for multiscale analysis of microfluidic filters. *J. Comput. Phys.* **178**, 342–372 (2002).

64. R. Roveda, D. B. Goldstein, P. L. Varghese, Hybrid Euler/direct simulation Monte Carlo calculation of unsteady slit flow. *J. Spacecr. Rockets* **37**, 753–760 (2000).
65. S. T. O’Connell, P. A. Thompson, Molecular dynamics–continuum hybrid computations: a tool for studying complex fluid flows. *Phys. Rev. E* **52**, R5792–R5795 (1995).
66. J. Li, D. Liao, S. Yip, Coupling continuum to molecular-dynamics simulation: reflecting particle method and the field estimator. *Phys. Rev. E* **57**, 7259–7267 (1998).
67. N. G. Hadjiconstantinou, Hybrid atomistic–continuum formulations and the moving contact-line problem. *J. Comput. Phys.* **154**, 245–265 (1999).
68. E. G. Flekkoy, G. Wagner, J. Feder, Hybrid model for combined particle and continuum dynamics. *Europhys. Lett.* **52**, 271–276 (2000).
69. H. S. Wijesinghe, N. G. Hadjiconstantinou, Discussion of hybrid atomistic–continuum methods for multiscale hydrodynamics. *Int. J. Multiscale Comput. Eng.* **2**, 189–202 (2004).
70. H. S. Wijesinghe, R. D. Hornung, A. L. Garcia, N. G. Hadjiconstantinou, Three-dimensional hybrid continuum–atomistic simulations for multiscale hydrodynamics. *J. Fluids Eng.* **126**, 768–777 (2004).
71. T. Werder, J. H. Walther, P. Koumoutsakos, Hybrid atomistic–continuum method for the simulation of dense fluid flows. *J. Comput. Phys.* **205**, 373–390 (2005).
72. L. L. Baker, N. G. Hadjiconstantinou, Variance reduction for Monte Carlo solutions of the Boltzmann equation. *Phys. Fluids* **17**, 051703.1–051703.4 (2005).
73. E. Lauga, H. A. Stone, Effective slip in pressure-driven Stokes flow. *J. Fluid Mech.* **489**, 55–77 (2003).
74. F. W. Went, The size of man. *American Scientist* **56**, 400–413 (1968).
75. W. C. Tang, T.-C. Nguyen, R. T. Howe, Laterally driven polysilicon resonant microstructures. *Sensors and Actuators* **20**, 25–32 (1989).
76. C. Mastrangelo, C. H. Hsu, A simple experimental technique for the measurement of the work of adhesion of microstructures, in *Technical Digest IEEE Solid-State Sensors and Actuators Workshop*, pp. 208–212 (1992).
77. L.-S. Fan, Y.-C. Tai, R. S. Muller, Integrated movable micromechanical structures for sensors and actuators. *IEEE Transactions on Electronic Devices* **35**, 724–730 (1988).
78. L.-S. Fan, Y.-C. Tai, R. S. Muller, IC-processed electrostatic micromotors. *Sensors and Actuators* **20**, 41–47 (1989).
79. Y.-C. Tai, R. S. Muller, IC-processed electrostatic synchronous micromotors. *Sensors and Actuators* **20**, 49–55 (1989).
80. S. Brunauer, *Physical Adsorption of Gases and Vapours*, Oxford University Press (1944).
81. A. Majumdar, I. Mezic, Stability regimes of thin liquid films. *Microscale Thermophys. Eng.* **2**, 203–213 (1998).
82. A. Majumdar, I. Mezic, Instability of ultra-thin water films and the mechanism of droplet formation on hydrophilic surfaces. *J. Heat Transfer* **121**, 964–971 (1999).
83. J. N. Israelachvili, *Intermolecular and Surface Forces*, second edition, New York: Academic Press (1991).